JOURNAL OF THERMOPHYSICS AND HEAT TRANSFER
Vol. 12, No. 2, April–June 1998

Microscale Thermal Characterization for Two Adjacent Dielectric Thin Films

Chun-Ping Jen* and Ching-Chang Chieng†
National Tsing Hua University, Hsinchu 30043, Taiwan, Republic of China

Heat conduction in two adjacent layers of dielectric thin films are analyzed by solving an equation of phonon radiative transfer. In the present work, the physical model is derived with an equilibrium temperature at the imaginary black interface, so that the two layers can be linked. Moreover, the effective mean free path can be corrected by the phonon scattering rate on grain boundaries of imperfect interface. Chemical-vapor-deposited diamond layer on silicon is chosen as the structure of the test case. The studies found that the interface is a critical issue in microscale thermal characteristics; for example, a temperature jump at the interface characterizes the effective thermal conductivity on diamond film and influences the temperature level on the silicon substrates. Energy transmission to the other layer increases the temperature jump at the interface and lowers the temperature level on the silicon substrate without changing the phonon mean free path. The disorder interface with various grain structures increases the phonon scattering rate and shortens the effective mean free path significantly; therefore, the temperature gradient across the diamond film increases and the normalized temperature jump at the interface is decreased substantially.

Nomenclature

C = heat capacity
d = grain size
I = phonon intensity
k = thermal conductivity
N = number of atoms
q = heat flux
T = temperature
t = time
U = internal energy
V = phonon group velocity
α = energy transmission coefficient
η = grain boundary scattering strength
θ = Debye temperature
Λ = phonon mean free path
μ = cosine of the angle between the phonon propagation velocity and the x direction
τ = relaxation time
Ω = solid angle

Subscripts
D = defects or at Debye temperature
eff = effective quantity
G = grain
GB = grain boundary
i = medium i
j = medium j
S = at imaginary interface
U = Umklapp process
ω = spectral quantity

Superscripts
$+$ = positive direction, $0 < \mu < 1$
$-$ = negative direction, $-1 < \mu < 0$
0 = at equilibrium

Introduction

HIGH-DENSITY chips and high heat generation are the general trends in electronic devices, and the temperature of solid-state devices often determines the thermal performance; therefore, heat transport becomes a critical issue in their design of small length scale. Very thin films (100 Å ~ 100 μm) of dielectric materials are extensively used in electronic devices, and the microscale heat transfer in thin films attracts much attention. Examples include silicon-on-diamond (SOD) circuits, in which chemical-vapor-deposited diamonds are layered on silicon,[1] and a novel composite diamond–gallium arsenide substrate.[2] These films, with thickness between 0.1 and 5 μm, have the potential to change the thermal performance of electronic microstructures. Majumdar[3] showed that Fourier's law cannot be applied to analyze heat conduction in a regime of temperature and thickness of dielectric thin films. He developed an equation of phonon radiative transfer (EPRT), based on Boltzmann transport theory, to analyze the heat conduction in a single thin film, and concluded that heat conduction by lattice vibrations or phonons behaves like radiative transfer for the microscale regime. Majumdar's results[3] demonstrated that Fourier's law overpredicted the heat flux when the mean free path is comparable to the film thickness. Furthermore, he suggested an effective mean free path Λ_{eff} as a function of bulk mean free path Λ and film thickness L in determining the thermal conductivity. Flik and Tien[4] derived the free path components in the direction of transport by simple geometrical considerations, and obtained the reduced thermal conductivity in a given direction as the size effect. The analysis agreed well with a solution to the Boltzmann equation, and with experimental data on homogeneous films. However, this model of size effect as a result of boundary scattering did not consider the effect of grain boundaries, and did not agree with experimental data on films with grain sizes smaller than the film thickness. The grain structures shown in an electron micrograph[5] demonstrated irregular patterns, such as extreme cases of random and columnar grains. The particles or waves

Received June 5, 1997; revision received Aug. 22, 1997; accepted for publication Oct. 15, 1997. Copyright © 1997 by the American Institute of Aeronautics and Astronautics, Inc. All rights reserved.

*Ph.D. Candidate, Department of Nuclear Engineering and Engineering Physics, 101, Section 2, Kuang Fu Road. E-mail: d843102@oz.nthu.edu.tw.

†Professor, Department of Nuclear Engineering and Engineering Physics, 101, Section 2, Kuang Fu Road. E-mail: cchieng@ne.nthu.edu.tw. Senior Member AIAA.

would scatter differently as they traveled through these different-shaped interfaces. Phonons are responsible for heat conduction in the dielectric material, e.g., diamond, and are strongly influenced by the grain boundaries near the interface. Therefore, analysis, including the grain-boundary effect on the interface, is essential, particularly as regards interaction with the microscale effect of diamond layer.[6] Goodson et al.,[5] Touzelbaev and Goodson,[6] and Goodson et al.[7] lumped the interfacial effects to a single layer by the use of thermal boundary resistance, and solved the phonon transport equation using the diffusion approximation and a slip boundary condition. This solution method was derived by Chen and Tien[8] to calculate the effective thermal conductivity for conduction normal to homogeneous layers.

In the present study, the EPRT is employed to analyze thermal performance for both the very thin film and the adjacent substrate, including the interfacial effects. The temperature profiles in both layers are of interest as well as the temperature jump across the interface. Two major issues are analyzed and discussed in this paper: 1) the effect from energy transmission between two media, and 2) the roughness effect from to phonon scattering on grain boundaries. The test case in the present study uses the diamond layer deposited on a silicon substrate.

Physical and Mathematical Formulation

Heat transfer in a dielectric solid by lattice vibrations or phonons can be analyzed using the semiclassical Boltzmann equation. Majumdar[3] transformed it to an EPRT in the form

$$\frac{1}{V}\frac{\partial I_\omega}{\partial t} + \mu\frac{\partial I_\omega}{\partial x} = \frac{I_\omega^0[T(x)] - I_\omega}{V\tau(\omega, T)} \tag{1}$$

where I_ω represents the intensity of phonons with frequency ω and τ is the relaxation or the mean free time between scattering as a function of ω and T. I_ω^0 is the equilibrium intensity corresponding to a blackbody intensity at temperatures below the Debye temperature. The heat flux $q(x)$ can be obtained by the integration over frequency and solid angle as follows:

$$q(x) = \int_{\Omega=4\pi}\int_0^{\omega_D} \mu I_\omega(x, \omega, \Omega)\, d\omega\, d\Omega \tag{2}$$

For steady state, the phonon radiative equilibrium is achieved, so that $\nabla \cdot q = 0$. Furthermore, $I_\omega^0(T)$ can be approximated by assuming a condition of equilibrium at every frequency, then

$$I_\omega^0 = \frac{1}{2}\int_{-1}^{1} I_\omega\, d\mu \tag{3}$$

Integrating the preceding equation over all the frequencies, the U of phonons can be obtained[9]

$$U = \int_{\Omega=4\pi}\int_0^{\omega_D} \frac{I_\omega}{V}\, d\omega\, d\Omega \tag{4}$$

And the internal energy of phonons can be also expressed as a function of temperature, based on Debye theory[10]

$$U = 9Nk_BT\left(\frac{T}{\theta}\right)^3\int_0^{x_D} dx\,\frac{x^3}{e^x - 1} \tag{5}$$

where k_B is the Boltzmann constant. The upper limit in the integral x_D is defined as θ/T. Linking Eqs. (4) and (5), the equilibrium intensity function can be expressed as

$$I^0(T) = 2\pi\int_0^{\omega_D}\left(\int_{-1}^{1} I_\omega\, d\mu\right) d\omega = 9NVk_BT\left(\frac{T}{\theta}\right)^3\int_0^{x_D} dx\,\frac{x^3}{e^x - 1} \tag{6}$$

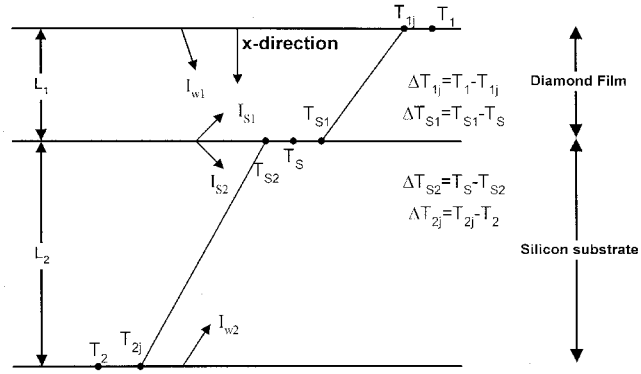

Fig. 1 Schematic diagram of two thin films.

The phonon internal energy function is proportional to the fourth power of temperature, when the temperature is much lower than the Debye temperature. If the temperature becomes higher, the phonon internal energy is proportional to the second power of temperature, and then linear proportional to temperature (present study).

Because the medium is assumed to be gray, the relaxation time is frequency independent. The subscript ω in Eq. (1) can be removed, i.e., the EPRT can be expressed as

$$\frac{1}{V}\frac{\partial I}{\partial t} + \mu\frac{\partial I}{\partial x} = \frac{\frac{1}{2}\int_{-1}^{1} I\, d\mu - I}{V\tau(T)} \tag{7}$$

These equations are applied to both media of the thin film and substrate.

Boundary and Interface Condition

The present study considers the thin film of thickness L_1 adjacent to the substrate of thickness L_2 (Fig. 1), with the x coordinate starting from the top surface of the diamond film. It is assumed that the boundaries at $x = 0$ and $L_1 + L_2$ are rough enough to scatter phonons diffusely, and the thermodynamic equilibrium is restored at these two surfaces. Therefore, the surface boundaries are black, with T_1 and T_2 under the Casimir limit. Conditions on the interface must be emphasized for the present study. Phonons in dielectric materials are scattered by boundaries, impurities, defects, and other phonons. The interface between the film and the substrate will either reflect or transmit phonons and act as a resistance to heat flow. The transmissivity will be discussed in the next section. The phonons reflected by the rough interface are assumed diffusely and the interface can reach local idealized thermodynamic equilibrium, i.e., the phonons are thermalized at the imaginary black interface with T_S.

While the intensities at the interface in the film side and in the substrate side are I_{S1} and I_{S2}, at the imaginary black interface

$$I_{S1} = I_1^0(T_S) \tag{8a}$$

$$I_{S2} = I_2^0(T_S) \tag{8b}$$

Although the temperature jumps at the interfaces as well as at the boundary surfaces are expected, the requirement of the constant heat flux across the two media must be met to validate this derivation.

If energy transmission across the interface is considered, the interface is not black but gray, and I_{S1} and I_{S2} can be expressed as

$$I_{S1} = (1 - \alpha_{1-2})I_1^+(L_1) + \alpha_{1-2}I_1^0(T_S) \tag{9a}$$

$$I_{S2} = (1 - \alpha_{2-1})I_2^-(L_1) + \alpha_{2-1}I_2^0(T_S) \tag{9b}$$

where α_{1-2} and α_{2-1} are the transmission coefficients at the interface from medium 1 to medium 2 and from medium 2 to medium 1, respectively. $I_1^+(L_1)$ is the radiation intensity at $x = L_1^-$ in the forward direction, that is, $0 < \mu < 1$, in medium 1, and $I_2^-(L_1)$ is the radiation intensity at $x = L_1^+$ in the backward direction, that is, $-1 < \mu < 0$, in medium 2.

Phonon Transmission Across the Interface

When phonons of a particular frequency are incident on the interface between two different media, only a fraction of energy is transmitted and the other fraction is reflected. For specular interface and constant heat capacity, Chen[11] derived the following relation to compute the energy transmission coefficient:

$$\alpha_{i-j}/\alpha_{j-i} = C_j V_j^3 / C_i V_i^3 \tag{10}$$

Real solid surfaces are usually rough, and the effect of roughness on transmission of phonons can be described by the effect of diffuse scattering on the thermal boundary resistance. Chen[12] derived the energy transmission coefficient for diffuse interface as follows:

$$\alpha_{i-j} = \frac{C_j V_j}{C_i V_i + C_j V_j} \tag{11}$$

The inelastic scattering is particularly significant at the interface formed by two solids having widely different Debye temperatures.[13] The work of Chen[12] pointed out that Eq. (11) automatically includes inelastic scattering. Furthermore, the values of specific heat and phonon velocity are employed.[14]

Interfacial Effect on Phonon Effective Relaxation Time in Thin Film

Because the crystalline of the substrate can be assumed to be perfect and the thickness of the substrate is usually much thicker than the thin film, size and/or disorder interfacial effect near the interface on the phonon mean free path are taken into account only for the film side. For the real interface, the τ for phonon scattering is required to solve the EPRT in Eq. (7) and is contributed by the phonon–phonon Umklapp scattering τ_U and the phonon scattering rate caused by defects such as impurities, grain boundaries, and rough interfaces τ_D, i.e.,

$$1/\tau = (1/\tau_U) + (1/\tau_D) \tag{12}$$

The effective relaxation time τ is the ratio of Λ and V, i.e., $\tau = \Lambda/V$, so that Eq. (12) can also be written as

$$\Lambda^{-1} = \Lambda_U^{-1} + \Lambda_D^{-1}$$

The relaxation time[15] for Umklapp processes is proportional to $[\omega^2 T^3 \exp(-\theta/aT)]^{-1}$, where a is a constant characteristic of the vibrational spectrum of the material. For diamond film, the relaxation time for Umklapp processes can be further expressed as[7]

$$[\tau_U(\chi_\omega, T)]^{-1} = A_U(\chi_\omega)^2 T^3 \exp[(-B_U)/T] \tag{13}$$

where $A_U = 640\ \mathrm{s}^{-1}\ \mathrm{K}^{-3}$ and $B_U = 470$ K. The dimensionless phonon frequency χ_ω is $\chi_\omega = h_P\omega/k_B T$, where h_P is Planck's constant divided by 2π.

Goodson[5] related the internal phonon scattering rate to d_G and to the dimensionless η. He assumed that the small grain dimension causes phonon scattering on defects near grain boundaries to dominate over scattering on defects within grain. This assumption leads $1/\tau_D$ in Eq. (12) to be replaced by the scattering rate from grain boundaries $1/\tau_{GB}$. Two approximations are proposed to relate $1/\tau_{GB}$ and d_G. Approximation 1 distributes the defects contributed by grain boundaries homogeneously within plane x, and approximation 2 collapses all of the imperfections onto the boundaries of grains. For approximation 1, the scattering rate is proportional to η and inversely proportional to d_G, i.e.,

$$[\tau_{GB}(d_G, \omega)]^{-1} = \frac{2V\eta(d_G, \omega)}{d_G} \tag{14}$$

For approximation 2, the scattering rate of phonons is an exponential function of grain-boundary scattering strength, which is appropriate for conduction normal to layers with an entirely columnar grain structure, i.e.,

$$[\tau_{GB}(d_G, \omega)]^{-1} = (2V/\pi d_G)\{1 - \exp[-(\pi/4)\eta(d_G, \omega)]\} \tag{15}$$

Λ_{GB} in both approximations are functions of d_G and ω. For a nonhomogeneous medium, the thermal boundary resistance R_T can be obtained as[8]

$$\frac{1}{R_T} = \frac{V}{3}\int_0^{\theta/T} \frac{C(\chi_\omega, T)\, d\chi_\omega}{d_E(\chi_\omega, T) + \frac{4}{3}[(1/\alpha_0) + (1/\alpha_{1-2}) - 1]} \tag{16}$$

where d_E is the dimensionless effective layer thickness calculated by

$$d_E(\chi_\omega, T) = \frac{1}{L_1}\int_0^{L_1} \frac{dz}{\Lambda_{GB}(z, \omega, T)} \tag{17}$$

The transmission coefficient α_{1-2} for phonons into the substrate ($x > L_1$) is calculated as discussed in the preceding paragraph, and the transmission coefficient α_0 on the top surface ($x = 0$) is set to 1 by the assumption of a black surface. $C(\chi_\omega, T)$ is the specific heat and is a function of phonon frequency and temperature.

Because the medium is assumed gray in the present work, an effective mean free path including grain boundary scattering is evaluated by

$$\bar{\Lambda}^{-1} = \frac{\displaystyle\int_0^{\theta/T} C(\chi_\omega, T)\, d\chi_\omega}{\displaystyle\int_0^{\theta/T} \frac{C(\chi_\omega, T)}{\Lambda^{-1}(\chi_\omega, T)}\, d\chi_\omega} \tag{18}$$

then $\tau = \bar{\Lambda}/V$ is obtained as the effective relaxation time and employed in EPRT.

Computational Method

The integral in Eq. (7) can be approximated by Gaussian quadrature

$$\int_{-1}^{1} I(\mu)\, du = \sum_{j=1}^{N} I(\mu_j) w_j$$

where μ_j are discrete directions and w_j are the weighting factors. Eight directions are recommended,[16] and 16 directions have been used to achieve the same results with good accuracy. Because the problem is solved under the assumption of radiative equilibrium, it was found that the heat flux maintained a constant along the computational domain. This was a way to verify whether the solution was correct.

Then, the two-flux model of radiative transfer[17] is applied to solve Eq. (7), i.e.,

$$\mu_j \frac{\partial I^+}{\partial x} = \frac{\frac{1}{2}\displaystyle\sum_{k=1}^{N} I(\mu_k) w_k - I^+}{V\tau} \quad \text{for } \mu_j > 0 \tag{19}$$

$$\mu_j \frac{\partial I^-}{\partial x} = \frac{\frac{1}{2}\displaystyle\sum_{k=1}^{N} I(\mu_k) w_k - I^-}{V\tau} \quad \text{for } \mu_j < 0 \tag{20}$$

These equations are discretized by the finite difference method. For radiation in forward directions, the backward difference is employed to calculate the first derivative of I^+ at location index i, i.e.,

$$\left.\frac{\partial I^+}{\partial x}\right|_i = \frac{I_i - I_{i-1}}{x_i - x_{i-1}} \tag{21}$$

For radiation in backward directions, the forward difference, instead of the backward difference, is used

$$\left.\frac{\partial I^-}{\partial x}\right|_i = \frac{I_{i+1} - I_i}{x_{i+1} - x_i} \tag{22}$$

Substituting Eqs. (21) and (22) into Eqs. (19) and (20), a set of difference equations can be formed

$$\mu_j \frac{I_{i,j} - I_{i-1,j}}{x_i - x_{i-1}} = \frac{\frac{1}{2}\sum_{k=1}^{N} I_{i,k} w_k - I_{i,j}}{V\tau} \quad \text{for } \mu_j > 0 \tag{23}$$

$$\mu_j \frac{I_{i+1,j} - I_{i,j}}{x_{i+1} - x_i} = \frac{\frac{1}{2}\sum_{k=1}^{N} I_{i,k} w_k - I_{i,j}}{V\tau} \quad \text{for } \mu_j < 0 \tag{24}$$

There are $NI1$ nodal points (i = 1 to $NI1$) in diamond film and $NI2$ nodal points ($i = NI1 + 1$ to $NI = NI1 + NI2$) in silicon substrate. The grids are clustered to the interface ($x = L_1$) to eliminate numerical error. There are $NI1$ (25) computational nodal points in medium 1 and additional $NI2$ (25) nodes in medium 2. There is no difference in the calculated intensities if finer grids ($NI1$ = 50, $NI2$ = 50) are employed. At the top surface of the diamond film (i = 1, x_1 = 0), $I^+_{1,j} = I^0_1(T_1)$. At the bottom surface of the silicon substrate ($x_{NI} = L_1 + L_2$), $I^-_{NI,j} = I^0_2(T_2)$. For the interface at $x_{NI1} = L_1^-$, $I^-_{NI,j} = I_{S1}$ in Eq. (9a); and at $x_{NI1+1} = L_1^+$, $I^+_{NI+1,j} = I_{S2}$ in Eq. (9b).

After the energy intensity at any location x_i and direction μ_j is obtained, the heat flux and temperature distribution are calculated by the following relations:

$$q(x_i) = 2\pi \sum_{j=1}^{N} \mu_j I_{i,j} w_j \tag{25}$$

$$I^0(T) = 2\pi \sum_{j=1}^{N} I_{i,j} w_j \tag{26}$$

Results and Discussions

Diamond has exceptional properties, such as high electrical resistivity, extreme hardness, and excellent conductivity of heat, and direct deposition of diamond on silicon is promising for achieving minimum thermal resistance between layers. Experimental data and computational predictions on thermal boundary resistance for diamond film are available to make comparisons with the present work. Therefore, the diamond layer deposited on silicon substrate is chosen as the demonstrating case in this study. Because the diamond film is much thinner than the base material of silicon, the emphasis will be put on the temperature profiles of the diamond film instead of the base material and the temperature slip at the interface. To illustrate the topping layer (medium 1), the EPRT is solved for different thicknesses of silicon vs different diamond layer thicknesses. Figure 2 shows that the decrease of diamond layer thickness reduces the effective thermal conductivity on the diamond film, and the curves for the silicon thicknesses of 10, 20, and 30 μm are coincided. Therefore, the following computations are performed with fixed thickness of 20 μm for medium 2. The effective thermal conductivity k_{eff} is defined as

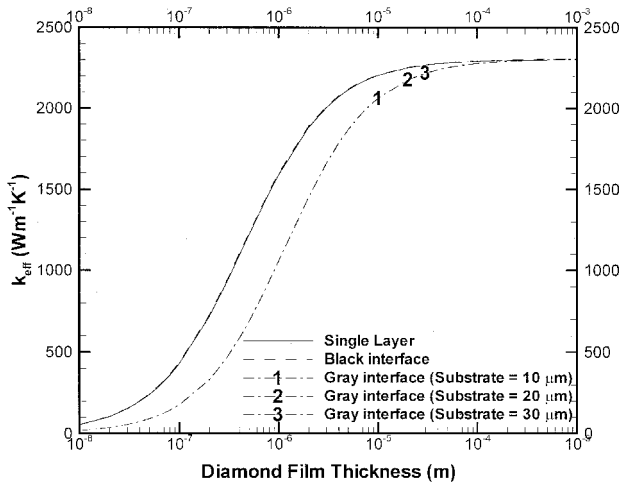

Fig. 2 Effective thermal conductivity for various film thicknesses of diamond and silicon.

$$k_{\text{eff}} = qL_1/(T_1 - T_S) \tag{27}$$

where q is the imposed heat flux on the topping surface.

Figure 2 also shows the film thickness effect on k_{eff} as well for comparison. Figure 2 demonstrates that the present method produces the same k_{eff} (dashed line), by treating the interface as a black surface, as the k_{eff} (solid line) by treating the single layer of diamond with two black boundary surfaces. The implementation of the transmission coefficient decreases the effective thermal conductivity. The reduction of effective thermal conductivity is caused by the enlargement of the temperature jump at the interface. When the film thickness is much larger than the phonon mean free path, the k_{eff} approaches bulk thermal conductivity. However, the k_{eff} approaches a constant of small value as the thickness approaches ultrathin thickness, because the phonon mean free path is limited to the physical dimension of the layer.

Figure 3 plots the normalized temperature distribution on the diamond film and the top portion of the silicon substrate. The normalized temperature is defined as

$$T_{\text{NORM}} = (T - T_2)/(T_1 - T_2) \tag{28}$$

Different magnitudes of temperature jump at the interface ($x = L_1$) and boundary surfaces (x = 0 and $L_1 + L_2$) are obtained for different assumptions with different diamond layer thicknesses. The temperature profiles and the jumps at the walls and at the interface are of interest in the present study.

Majumdar[3] treated the boundary surfaces of the diamond layer as black surfaces, based on the relative large ratio of the phonon mean free paths in the diamond and the silicon. Therefore, he solved the temperature profile in a single layer only, and his calculation is equivalent to the part of our solutions for the black-interface cases. The smallest temperature jumps and the highest temperature levels in silicon substrate are observed for this simplified case, which coincide with the solutions for a single-layer assumption. The temperature jump is enlarged when the energy transmissions from the other sides are taken into account, and are calculated by the equation derived by Chen,[12] i.e., $\alpha_{1-2} = 0.33$ and $\alpha_{2-1} = 0.67$ in the present case. This is because a fraction of incident energy is reflected at the interface, that is, the thermal resistance at the interface increases. It is observed that the temperature distributions on the diamond layer with a thickness of 5 μm are almost the same for both black and gray interfaces, and the temperature level of the substrate is lower by the layer temperature jump

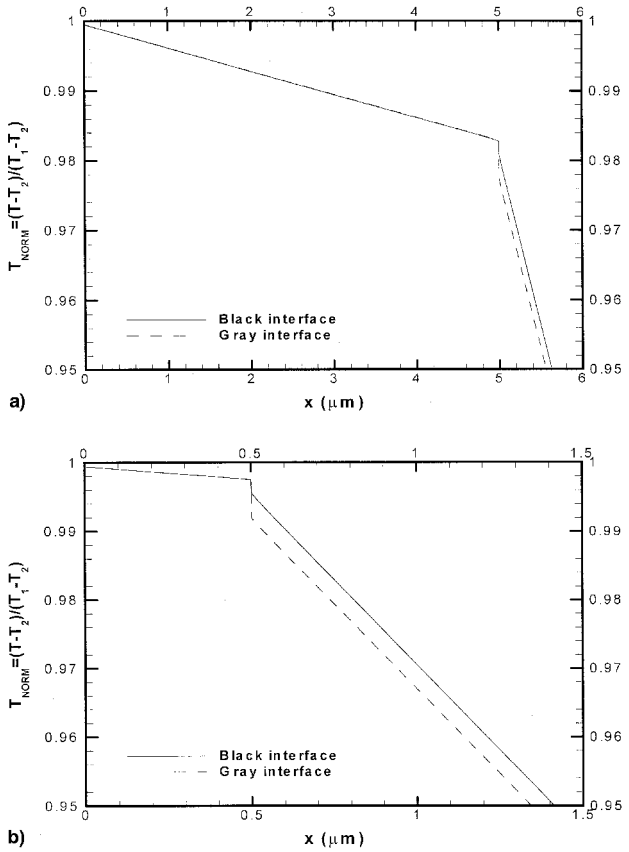

Fig. 3 Temperature profiles on diamond–silicon films. Diamond film thickness = a) 5 and b) 0.5 μm.

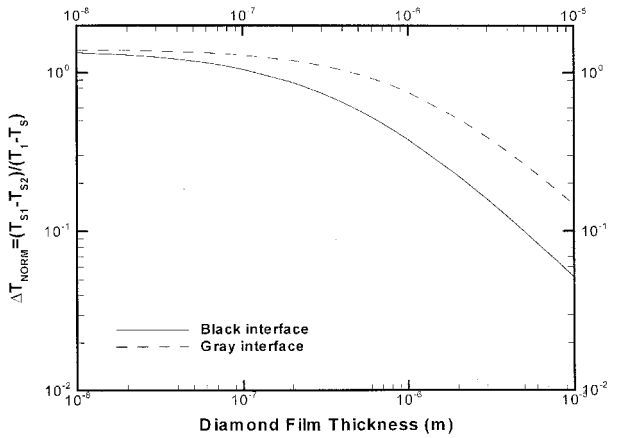

Fig. 4 Energy transmission on normalized temperature jumps.

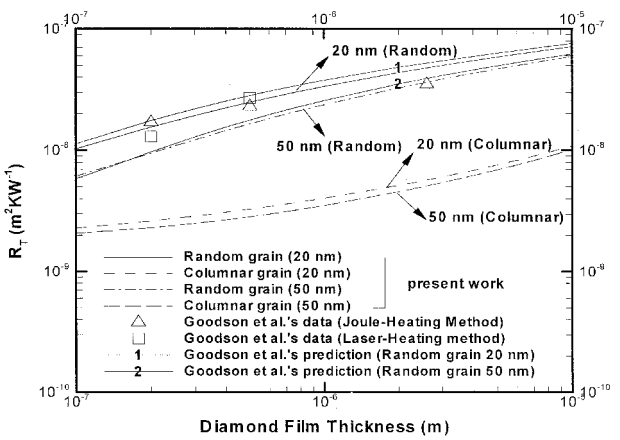

Fig. 5 Thermal boundary resistance vs diamond film thickness for grain sizes and structures at interface.

for the gray interface (Fig. 3a), compared with the level for the black interface. As the film thickness is reduced to 0.5 μm (Fig. 3b), the temperature is more uniform in the diamond film and higher on average than the temperature for the 5-μm thickness. In addition, the temperature jumps at the interface in Fig. 3b are larger than those shown in Fig. 3a because of a thinner film thickness.

Figure 4 concludes the effects mentioned in the preceding text on the normalized temperature jump by $\Delta T_{NORM} = \Delta T_{jump}/(T_1 - T_S)$, where T_S is the idealized temperature at the imaginary black interface. For the black interface case, the normalized temperature jump is equivalent to that obtained by single-layer approximation, which is shown by the bottom line. These curves illustrate that the normalized temperature jump increases as the layer thickness decreases. The increase rate slows as the film thickness approaches the phonon mean free path. The temperature jump approaches a constant as the layer thickness approaches this limit. As the phonon transmission between the two media is implemented, the normalized temperature jump is larger than that of the black surface for all of the film thickness from 10^{-5} to 10^{-8} m. The increases in temperature jump are contributed by the changes of layer thickness in the diamond and the ratio of the diamond-to-silicon layer thicknesses.

Because the deposition of film diamond layers on silicon forms a highly irregular interface, the scattering rate of the phonons is strongly influenced by grain size and boundaries. The phonon mean free path and thus the effective thermal conductivities of diamond are significantly altered, which will affect the temperature distributions on both layers and the temperature jump at the interface. Goodson et al.[7] measured the total thermal resistance for conduction normal to diamond layers thinner than 5 μm on silicon substrate, and obtained the prediction of thermal boundary resistance using the same analogy as solving equivalent phonon transport equations (Eq. 16), as discussed in the preceding sections. Figure 5 plots the predicted thermal boundary resistance vs diamond layer thickness by the present computational method. The agreements between the data of Goodson et al.[7] and the present predictions are achieved. It is evidence that verifies the present computation. An effective silicon–diamond boundary resistance resulted from the high rate of phonon scattering within the diamond near the interface.[7] The thermal boundary resistance of the randomly oriented grains at the interface increases 1.2–1.5 times, as the size of the same grain structure is decreased from 50 to 20 nm, but the resistance is not altered much for different sizes of grain with columnar grain structure. However, significant differences in resistances for different grain structures are obtained. Although measured data agree with predicted values by randomly oriented grains, it is interesting to detail the thermal performance with different grain structures. Additional information on temperature profiles on both media and temperature jump at the interface can be provided by the present computational model.

Figure 6a shows the normalized temperature profiles on both media, with a diamond thickness of 5 μm and a silicon thickness of 20 μm, and a 20-nm grain size at the interface. The top solid line is obtained by the classical Fourier's law, which indicates the most uniform temperature distribution in diamond layer and the highest temperature levels in silicon substrate among all curves. If the grains at the interface are randomly oriented, the temperature gradient in the diamond layer is largely increased, as shown in the bottom two curves. The line next to the top line (Fig. 6a) shows that there is a small temperature jump at the interface, which results from the black-interface assumption. The temperature jump is enlarged as the interface is assumed to be gray, which results from the same

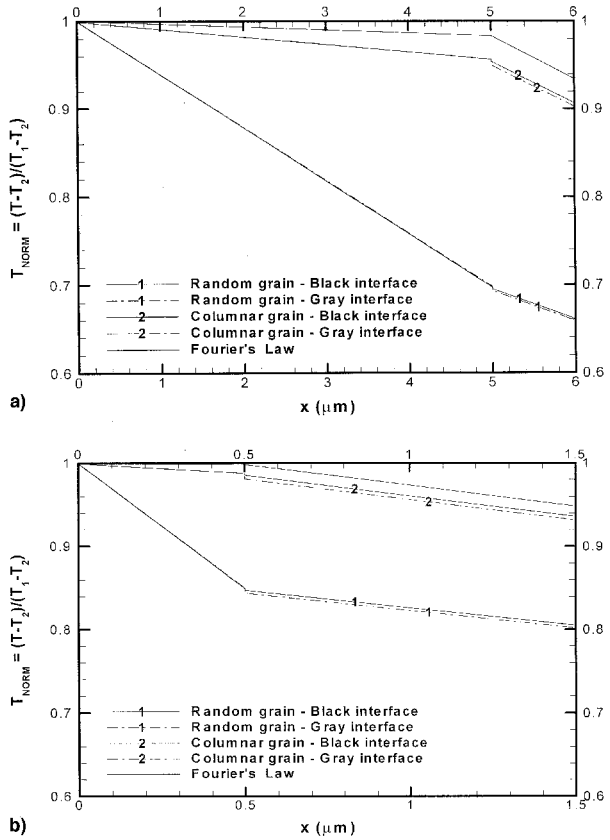

Fig. 6 Temperature profiles on diamond–silicon films with same grain size (20 nm) at interface but different grain structure. Diamond film thickness = a) 5 and b) 0.5 μm.

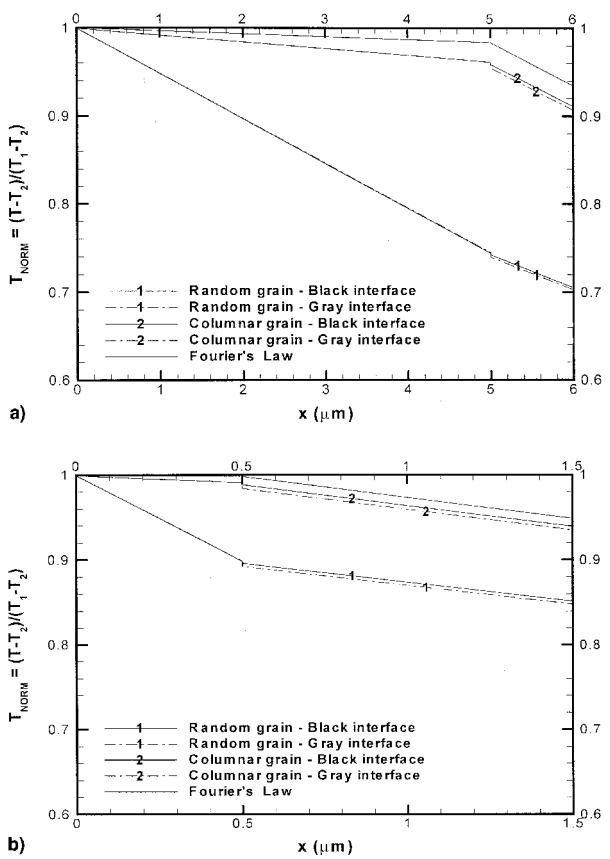

Fig. 7 Temperature profiles on diamond–silicon films with same grain size (50 nm) at interface but different grain structure. Diamond film thickness = a) 5 and b) 0.5 μm.

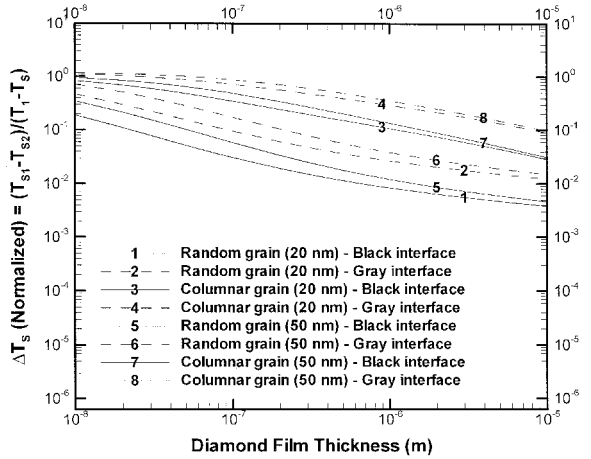

Fig. 8 Normalized temperature jump vs diamond film thickness for different grain sizes and structures at interface.

reasons as for a perfect (no scattering on grain boundary) interface with energy transmission. The temperature jump at the interface, considering phonon scattering on the grain boundary, is slightly smaller than that with the perfect interface because of a smaller phonon mean free path (Fig. 3a). In the meantime, the temperature gradient across the diamond layer of Fig. 3 is much larger (~15 times) than that with the perfect interface. This is because of much shorter phonon mean free paths from scattering on grain boundaries leading to much smaller effective thermal conductivity. A large temperature gradient across the diamond layer implies smaller effective thermal conductivity and larger thermal boundary resistance.

If the grain is columnar structured, the phonon mean free path is on the order of hundreds of nanometers, which is comparable to the bulk mean free path. Therefore, the temperature gradient across the film is effectively reduced (Fig. 6), but its magnitude is still higher than those with perfect interface (Fig. 3). As the diamond film is reduced, the temperature jump at the interface is enlarged (Figs. 6a and 6b).

If the grain size is 50 nm at the interface, the thermal boundary resistance is lowered (Fig. 5), which implies higher effective thermal conductivity and a flatter temperature gradient on the diamond film (comparing Figs. 6 and 7). A flatter temperature profile on the diamond layer also indicates a higher temperature level on the silicon substrate. Figure 8 plots the normalized temperature jump at the interface vs the diamond film thickness for different grain sizes and structures at the interface. Although the thinner diamond film still implies larger increases of the normalized temperature jump, as the perfect interface demonstrates, the increasing rates of jump magnitude are changed (comparing Figs. 4 and 8). Moreover, the following facts are illustrated:

1) The temperature jump with the randomly oriented grain is much lower than the jump with the columnar-structured grain.

2) Larger grain size implies a slightly higher temperature jump at the interface.

3) The grain size dependency is stronger for randomly oriented grains than for columnar-structured grains because the phonon mean free path is a weaker function of film thickness than for columnar-structured grains.

Conclusions

The present study extends the EPRT to calculate the thermal performance for two adjacent dielectric thin films by introducing an equilibrium temperature at the imaginary black interface and the effective mean free path. Therefore, the temperature profile on both media and the temperature jump across the interface can be obtained simultaneously. Based on the

demonstrating case of the chemical-vapor-deposited diamond layer on silicon, the major findings are as follows:

1) Thinner diamond film implies lower effective thermal conductivity, a larger temperature slip on the diamond surface, and a larger temperature jump at the interface. The trends are the same as those for a single layer of diamond film.

2) When the interface is assumed to be black, all of the incident energy is absorbed and no energy is reflected. As the gray interface is implemented, that is, the transmission of energy is calculated, the temperature jump at the interface is enlarged because of the energy reflected, i.e., the increase in thermal boundary resistance at the interface, and the temperature level in the silicon substrate is lowered.

3) Disorder interfaces with randomly oriented grain or columnar-structured grain increase the phonon scattering rate and dominate the thermal performance of the diamond film and silicon substrate. The interface with a column-structured grain provides much better thermal performance than the interface with a randomly oriented grain.

References

[1]Ravi, K. V., and Landstrass, M. I., "Silicon on Insulator Technology Using CVD Diamond," *Proceedings of the 1st International Symposium on Diamond and Diamond-Like Films*, The Electrochemical Society, Pennington, NJ, 1989, pp. 24–37.

[2]Goodson, K. E., Kurabayashi, K., and Pease, R. F. W., "Improved Heat Sinking for Laser-Diode Arrays Using Microchannels in CVD Diamond," *Proceedings of the ASME National Heat Transfer Conference* (Portland, OR), Vol. 3, American Society of Mechanical Engineers, New York, 1995, pp. 187–192.

[3]Majumdar, A., "Microscale Heat Conduction in Dielectric Thin Films," *Journal of Heat Transfer*, Vol. 115, Feb. 1993, pp. 7–16.

[4]Flik, M. I., and Tien, C. L., "Size Effect on the Thermal Conductivity of High-T_c Thin-Film Superconductors," *Journal of Heat Transfer*, Vol. 112, Nov. 1990, pp. 872–881.

[5]Goodson, K. E., "Thermal Conduction in Nonhomogeneous CVD Diamond Layers in Electronic Mictrostructures," *Journal of Heat Transfer*, Vol. 118, May 1996, pp. 279–286.

[6]Touzelbaev, M. N., and Goodson, K. E., "Impact of Nucleation Density on Thermal Resistance near Diamond-Substrate Boundaries," *Proceedings of the 31st ASME National Heat Transfer Conference* (Houston, TX), Vol. 5, American Society of Mechanical Engineers, New York, 1996, pp. 193–200.

[7]Goodson, K. E., Käding, O. W., Rösler, M., and Zachai, R., "Experimental Investigation of Thermal Conduction Normal to Diamond-Silicon Boundary," *Journal of Applied Physics*, Vol. 77, Feb. 1995, pp. 1385–1391.

[8]Chen, G., and Tien, C. L., "Thermal Conductivities of Quantum Well Structures," *Journal of Thermophysics and Heat Transfer*, Vol. 7, No. 2, 1993, pp. 311–318.

[9]Tzou, D. Y., *Macro- to Microscale Heat Transfer*, Taylor and Francis, Washington, DC, 1997, Chap. 1.

[10]Kittel, C., *Introduction to Solid State Physics*, Wiley, New York, 1986, Chap. 5.

[11]Chen, G., "Size and Interface Effects on Thermal Conductivity of Superlattices and Periodic Thin-Film Structures," *Proceedings of the 31st ASME National Heat Transfer Conference* (Houston, TX), Vol. 1, American Society of Mechanical Engineers, New York, 1996, pp. 121–129.

[12]Chen, G., "Heat Transport in the Perpendicular Direction of Superlattices and Periodic Thin-Film Structures," *Proceedings of the ASME International Mechanical Engineering Congress and Exposition* (Atlanta, GA), Micro-Electro-Mechanical Systems (MEMS), Dynamic Systems and Control Div., Vol. 59, American Society of Mechanical Engineers, New York, 1996, pp. 13–24.

[13]Stoner, R. J., and Maris, H. J., "Kapitza Conductance and Heat Flow Between Solids at Temperatures from 50 to 300 K," *Physical Review B: Solid State*, Vol. 48, No. 22, 1993, pp. 16,373–16,387.

[14]Chen, G., "Nonlocal and Nonequilibrium Heat Conduction in the Vicinity of Nanoparticles," *Journal of Heat Transfer*, Vol. 118, 1996, pp. 539–545.

[15]Callaway, J., "Model for Lattice Thermal Conductivity at Low Temperatures," *Physical Review*, Vol. 113, No. 4, 1959, pp. 1046–1051.

[16]Kumar, S., Majumdar, A., and Tien, C. L., "The Differential-Discrete Ordinate Method for Solving the General Equation of Radiative Transfer," *Journal of Heat Transfer*, Vol. 112, May 1990, pp. 424–429.

[17]Siegel, R., and Howell, J. R., *Thermal Radiation Heat Transfer*, McGraw–Hill, New York, 1981, Chaps. 14, 15.